Atmospheric and Climate Sciences, 2011, 1, 19-32
doi: 10.4236/acs.2011.12003 Published Online April 2011 (http://www.SciRP.org/journal/acs)

An Examination of the Effects of Aerosol Chemical Composition and Size on Radiative Properties of Multi-Component Aerosols

Shaocai Yu*, Yang Zhang
Department of Marine, Earth, and Atmospheric Sciences, North Carolina State University, Raleigh, USA
E-mail:yu.shaocai@epa.gov
Received

Abstract

The sensitivity of aerosol radiative properties (i.e., scattering coefficient, extinction coefficient, single scatter albedo, and asymmetry factor) and radiation transmission to aerosol composition, size distributions, and relative humidity (RH) is examined in this paper. Mie calculations and radiation calculations using a tropospheric visible radiation model are performed. The aerosol systems considered include inorganic and organic ions (e.g., Cl^-, Br^-, NO_3^-, SO_4^{2-}, Na^+, NH_4^+, K^+, Ca^{2+}, Mg^{2+}, $HCOO^-$, CH_3COO^-, $CH_3CH_2COO^-$, CH_3COCOO^-, $OOCCOO^{2-}$, MSA^{1-}), and (2) water-insoluble inorganic and organic compounds e.g., (black carbon, *n*-alkanes, SiO_2, Al_2O_3, Fe_2O_3 and other organic compounds). The partial molar refraction method and the volume-average method are used to calculate the real and imaginary parts of refractive index of real aerosols, respectively. The sensitivity simulations show that extinction coefficient increases by 70% when RH varies from 0 to 80%. Both extinction coefficient and asymmetry factor increase by ~48% when real part varies from 1.40 to 1.65. Scattering coefficient and single scattering albedo decrease by 18% and 24%, respectively, when the imaginary part varies from –0.005 to –0.1. Scattering and extinction coefficients increase by factors of 118 and 123, respectively, when the geometric mean radius varies from 0.05 to 0.3 μm. Scattering and extinction coefficients and asymmetry factor increase by factors of 389, 334, and 5.4, respectively, when geometric standard deviation varies from 1.2 to 3.0. The sensitivity simulations using a tropospheric visible radiation model show that the radiation transmission is very sensitive to the change in geometric mean radius and standard deviation; other factors are insignificant.

Keywords: Radiative Properties, Sensitivity Study, Aerosol Composition, Aerosol Size Distribution, Multi-Component Aerosols

1. Introduction

Atmospheric aerosols may influence the Earth's radiation balance directly by backscattering and absorption of solar radiation, and indirectly by increasing cloud condensation nuclei (CCN) concentrations, which in turn increase cloud droplet concentrations and thus backscattering of solar radiation [1-3]. The IPCC [4] concluded that increasing concentrations of the long-lived greenhouse gases have led to a combined radiative forcing +2.63 [± 0.26] $W \cdot m^{-2}$, and the total direct aerosol radiative forcing is estimated to be –0.5 [± 0.4] $W \cdot m^{-2}$, with a *medium-low* level of scientific understanding, while the radiative forcing due to the cloud albedo effect (also referred to as the first indirect effect), is estimated to be –0.7 [–1.1, +0.4] $W \cdot m^{-2}$, with a *low* level of scientific understanding. Evaluation of aerosol direct radiative forcing is complicated by the fact that aerosols are highly and non-uniformly distributed over the Earth and comprise a variety of chemical species, and their abundance varies with particle size, location and time. As indicated by Penner *et al*. [5], one of central scientific questions related to the direct radiative influence of aerosols is how the aerosol composition and size distributions affect the optical depth and radiative properties of aerosols, including dependence

Copyright © 2011 SciRes.

on relative humidity. Up to today the sensitivity of direct aerosol forcing to chemical composition, size distribution and relative humidity on a global scale has been tested with a "reference box model" [1] and a GCM model [6-8] Most of these studies except for Jacobson (2001) on direct aerosol forcing only focused on anthropogenic sulfate aerosols. The objectives of this paper are (1) to accurately calculate the refractive index of aerosol particles with the known chemical composition of atmospheric aerosol; (2) to theoretically evaluate the sensitivity of aerosol radiative properties and radiation transmission in the visible range to refractive index, size distributions, and relative humidity (RH) using a box model that includes Mie and radiative transfer calculation. Since the aerosol particle refractive index is determined by its chemical composition, the dependence of radiative properties of aerosol particles on the refractive index can indicate the effects of chemical composition. Since most of the light scattering and extinction are caused by particles in the accumulation mode size range (0.1 - 1.0 μm, diameter), and these particles are neither removed effectively by impaction nor by diffusion, the accumulation mode particles are the most important one in terms of aerosol radiative forcing. In this study the sensitivity of aerosol radiative properties to size distribution is examined on the basis of the calculation of the particle radiative properties for the accumulation mode only.

2. Model Formulation

2.1. Atmospheric Aerosol Composition and Size Distribution

Atmospheric aerosol particles are composed of complex mixtures of natural and anthropogenic chemical species that include (1) water-soluble inorganic and organic compounds such as sulfate, nitrate, formate and acetate, (2) water-insoluble inorganic and organic compounds such as black carbon, Al_2O_3 and *n*-alkanes, and (3) water itself. Soluble individual anion and cation concentrations of atmospheric aerosol are typically measured by Ion Chromatography (IC), and elements such as Al and Pb are determined by partially induced X ray emission (PIXE). On the other hand, the concentrations of insoluble high molecular weight organic compounds in aerosols are measured by gas-chromatography-masss pectrometer (GS/MS) method [9]. The IC and PIXE methods provide no information on the concentrations of specific salts or classes of inorganic and organic salts. The GC/MS method can quantify the concentrations of individual organic compounds in atmospheric particles. However, only about 10% of the total organic mass can be typically identified by the GC/MS method [9. In general, the water-soluble materials within atmospheric aerosol particles are expected to be a mixture of different chemicals and the water soluble parts of aerosol particles are considered to be a mixture of electrolytes together with any other water-soluble material. There are possible interactions between those ions that do not commonly exist between chemical components, especially at high RH conditions [10]. For example, in a mixture of KNO_3 and NaCl, there is a possible interaction between K^+ and Na^+. It is therefore reasonable to consider water-soluble parts of aerosol particles as a mixed solute, and aerosol particles at a dry state composed of mixed solute and insoluble substances. Since the composition of the aerosol particles depends on the sources and subsequent transformation while airborne, it is possible to separate aerosols into urban, rural continental and marine aerosols in a first approximation [11]. **Table 1** provides the estimates of refractive index of chemical components for the three atmospheric aerosol types. The concentrations of inorganic compounds (Cl^-, Br^-, NO_3^-, SO_4^{2-}, Na^+, NH_4^+, K^+, Ca^{2+}, Mg^{2+}, SiO_2, Al_2O_3, and Fe_2O_3), total concentrations of organics, and total mass concentrations of aerosol particles for three aerosol types were taken from the estimates of Pueschel [11]. For organics, over 80 individual organic compounds found in aerosol particles were identified and quantified previously [9]. In this study, the concentrations of soluble organic compounds ($HCOO^-$, CH_3COO^-, $CH_3CH_2COO^-$, CH_3COCOO^-, $OOCCOO^{2-}$, Methane sulfonic acid (MSA)) were taken from the estimates of Yu [2]. Chylek *et al*. [12] showed that the average black carbon (BC) atmospheric concentration in the continental air was 0.23 ± 0.04 μg/m^3 compared with 0.03 ± 0.01 μg/m^3 for the maritime air in the measurements over the southern Nova Scotia. Huntzicker *et al*. [13] indicated that the average BC concentration for 26 cities in the United State was 3.8 μg/m^3. In this study, the BC concentrations used for urban, continental, and marine aerosols are 3.8, 0.23 and 0.06 μg/m^3, respectively. The other organic compound concentrations listed in **Table 1** were taken from the estimates of Roggie *et al*. [9]. **Table 2** lists the physical chemical and optical properties of various pure salts in atmospheric particles. For the aerosol model computation, a lognormal distribution function is suitable to characterize the size distribution of atmospheric aerosols [11]. Particles in the accumulation mode (0.1 - 1.0 μm, aerodynamic diameter) are the most important one in terms of aerosol radiative forcing. **Table 3** lists the typical size distributions for three types of aerosol for the accumulation mode at a dry state compiled from literatures. As shown, the total number concentration, the geometric mean diameter (D_g), and the geometric standard devia-

Copyright © 2011 SciRes.

Table 1. The aerosol chemical composition under different environments and their calculated refractive index (real part) (see text for explanation).

Species	Aerosol type (μg/m^3)		
	Urban	Continental	Marine
Soluble component			
OH^-	0	0	0
F^-	0	0	0
Br^-	0.1	0.02	0.02
Cl^-	3.2	0.11	4.6
NO_3^-	3	0.9	0.05
SO_4^{2-}	14	2.8	2.6
Na^+	1.2	0.05	2.9
NH_4^+	4.8	1.2	0.16
K^+	0.4	0.06	0.1
Ca^{2+}	1.6	0.17	0.2
Mg^{2+}	0.6	0.09	0.4
$HCOO^-$	0.108	0.045	0.025
CH_3COO^-	0.118	0.018	0.01
$CH_3CH_2COO^-$	0	0	0
$CH_3(CO)COO^-$ (pyruvic)	0	0	0
$(OOCCOO)^{2-}$ (oxalic)	0.158	0.015	0.015
$CH_3S(O)_2OH$ (MSA)	0.008	0.008	0.008
Insoluble component			
BC (balck carbon)	3.8	0.23	0.06
SiO_2	5.9	0.7	0
Al_2O_3	3.6	0.24	0
Fe_2O_3	5.3	0.22	0.07
$CH_3(CH_2)_{14}COOH$(n-Hexadecanoic acid)	0.118	0.014	0.014
$CH3(CH2)_{16}COOH$(n-Octadecanoic acid)	0.057	0.002	0.002
$HOOCCH_2COOH$(Malonic acid)	0.028	< 0.00001	< 0.00001
$HOOC(CH_2)_2COOH$(Succinic acid)	0.055	< 0.00001	< 0.00001
$HOOC(CH_2)_3COOH$(Glutaric acid)	0.028	< 0.00002	< 0.00002
$C_6H_4(COOH)_2$(1,2-Benzenedicarxylic acid)	0.06	< 0.00002	< 0.00002
other organic compounds	26	0.9	0.8
Total organic mass (μg/m^3)	30.6	1.17	0.9
Total inorganic mass (μg/m^3)	43.5	6.4	11.2
Total mass (μg/m^3)	74.24	7.79	12.03
Mean density (μg/m^3)	1.82	1.89	1.825
Refractive index for aerosol particles	1.59	1.564	1.479

tion (σ_g) for the accumulation mode are in the ranges of 18.6 to 3000 cm^{-3}, 0.076 to 0.75 μm, and 1.35 to 2.0, respectively.

2.2. The Effect of Relative Humidity

Table 2 lists the RH at which the deliquescence will occur for some pure salts (RHD). The effects of continuously increasing RH on the growth of a pure salt aerosol particle can be calculated from equilibrium thermodynamics [10]. However, it is very difficult to predict this so-called "hysteresis effects" of water uptake for actual multi-component aerosol particles because this not only depends on the history of RH but also varies from one sample to another [10]. Here, the particle hysteresis effects should not be considered in detail. Instead, the den-

Copyright © 2011 SciRes.

Table 2. The physical-chemical and optical properties of different salts in atmospheric aerosol particles. RHD is the RH of deliquescence (see text for explanations).

Salts	Refractive Index	Density ($g \cdot cm^{-3}$)	RHD(%)	Salts	Refractive Index	Density ($g \cdot cm^{-3}$)	RHD (%)
NH_4CH_3COO		1.174		$Mg(CH_3COO)_2(H_2O)_4$	1.491	1.454	
NH_4Br	1.712	2.429		$MgBr_2$		3.724	
NH_4HCO_3	1.423	1.580		$MgCO_3$	1.717	2.958	
NH_4Cl	1.642	1.527	80	$MgCO_3(H_2O)_5$	1.456	1.730	
NH_4F		1.009		$MgCl_2$	1.675	2.320	
NH_4NO_3		1.725	62	$MgCl_2(H_2O)_6$	1.495	1.569	
$(NH_4)_2SO_4$	1.521	1.769	80	$Mg(NO_3)_2(H_2O)_6$		1.636	
NH_4HSO_4	1.473	1.780	40	$MgSO_4$	1.560	2.660	
$Ca(CH_3COO)_2$	1.550			$MgSO_4(H_2O)_7$	1.433	1.680	
Ca(Br)		3.353		$MgSO_4(H_2O)$	1.523	2.445	
$CaCO_3$	1.658	2.710		KBr	1.559	2.750	84
$CaCO_3(H_2O)_6$	1.460	1.771		K_2CO_3	1.531	2.428	43
$CaCl_2$	1.520	2.150	32	$K_2CO_3(H_2O)_2$	1.380	2.043	43
$CaCl_2(H_2O)_6$	1.417	1.710		$KHCO_3$	1.482	2.170	
$Ca(HCOO)_2$	1.510	2.015		KCl	1.490	1.984	88
$Ca(NO_3)_2(H_2O)_4$	1.465	1.896		KF	1.363	2.480	
$CaSO_4$	1.505	2.610		$KF(H_2O)_2$	1.352	2.454	
$CaSO_4(H_2O)_2$	1.521	2.320		K_2SO_4	1.494	2.662	
$NaCH_3COO$	1.464	1.528	78	$KHSO_4$	1.480	2.322	86
NaBr	1.641	3.203	58	Pb	2.010	11.344	
Na_2CO_3	1.535	2.532	90	BC	2.000	2.250	
$Na_2CO_3(H_2O)_{10}$	1.405	1.440		O_3	1.223		
$NaHCO_3$	1.500	2.159		SiC	2.654	3.217	
NaCl	1.544	2.165	75.3	SiO_2	1.487	2.320	
NaF	1.336	2.558		$H_2SO_4(H_2O)_2$	1.405		
$NaNO_3$	1.587	2.261	74.5	$PbCl_2$	2.199	5.850	
Na_2SO_4	1.484	2.680	84	Fe_2O_3	3.220	5.240	
$Na_2SO_4(H_2O)_{10}$	1.394	2.680	84	Al_2O_3	1.768	3.965	
$NaHSO_4(H_2O)$	1.460	2.476	52	PbO	2.510	8.000	
CH_3CHO	1.332	0.783		H_2O	1.333	1.000	
$CH_3(CH_2)_{14}COOH$	1.433	0.853		$CH_3(CH_2)_{14}COOH$	1.434	0.853	
$CH_3(CH_2)_{16}COOH$	1.422	0.941		formic acid	1.371	1.220	
$HOOCCH_2COOH$		1.619		acetic acid	1.372	1.049	
$HOOC(CH_2)_2COOH$	1.450	1.572		pyruvic acid	1.428	1.227	
$HOOC(CH_2)_3COOH$	1.419	1.424		oxalic acid		1.900	
$C_6H_4(COOH)_2$	1.431	1.462					
Other organics	1.550	1.400					

sity, refractive index, and radius of aerosol particles are considered as a unique function of RH in which the "hysteresis effects" are partially taken into account for three aerosol types using the experimental data of Hänel [10]:

$$\rho = \rho_w + (\rho_0 - \rho_w)\left(1 + \frac{\rho_0}{\rho_w}\bar{\mu}\frac{RH}{1-RH}\right)^{-1} \quad (1)$$

Copyright © 2011 SciRes.

Table 3. Scattering and extinction coefficients, asymmetry factor and single scattering albedo and their growth factor for selected aerosol types. Scattering coefficient (σ_{sp}, km^{-1}), extinction coefficient (σ_{ep}, km^{-1}), asymmetry factor (g) and single scattering albedo (ω). The indices 1,2,3 represent the values at RH=30%, 80% and 99%, respectively. Read $\frac{\sigma_{sp2}}{\sigma_{sp1}}$ as ratio of scattering coefficient at RH = 80% to that at RH = 30%.

Spectrum	Aerosol types	Accumulation mode			Scattering coefficient		extinction coefficient		asymmetry factor		single scattering albedo	
		n (cm^{-3})	D_g (μm)	σ_g	$\frac{\sigma_{sp2}}{\sigma_{sp1}}$	$\frac{\sigma_{sp3}}{\sigma_{sp1}}$	$\frac{\sigma_{ep2}}{\sigma_{ep1}}$	$\frac{\sigma_{ep3}}{\sigma_{ep1}}$	$\frac{g_2}{g_1}$	$\frac{g_3}{g_1}$	$\frac{\omega_2}{\omega_1}$	$\frac{\omega_3}{\omega_1}$
Meszaros [25]	Urban	560	0.1	2	1.89	20.76	1.78	18.22	1.12	1.26	1.06	1.14
Whitby [30]	Continental	2300	0.076	2	1.72	14.99	1.66	13.8	1.11	1.29	1.04	1.09
Hoppel *et al* [26]	Continental	3000	0.08	2	1.71	14.47	1.65	13.34	1.11	1.28	1.04	1.09
Leaitch and Isaac [31]	Continental	1000	0.24	1.35	1.74	16.76	1.68	15.57	1.14	1.39	1.03	1.08
Jenning *et al* [32]	Continental-marine mixture	950	0.2	1.35	1.82	21.52	1.75	19.75	1.18	1.53	1.04	1.09
Gathman [27]	Maritime	67	0.266	1.62	1.92	16.41	1.9	16.08	1.12	1.35	1.01	1.02
Jaenicke and Schutz [33]	Polar aerosol	18.6	0.75	2	1.57	5.53	1.55	5.37	1.06	1.1	1.01	1.03
Average		1127	0.24	1.76	1.77	15.78	1.71	14.59	1.12	1.32	1.03	1.08

$$m_r = m_{rw} + (m_{r0} - m_{rw})\left(1 + \frac{\rho_0}{\rho_w}\bar{\mu}\frac{RH}{1-RH}\right)^{-1} \quad (2)$$

$$m_i = m_{iw} + (m_{i0} - m_{iw})\left(1 + \frac{\rho_0}{\rho_w}\bar{\mu}\frac{RH}{1-RH}\right)^{-1} \quad (3)$$

$$r = r_0\left(1 + \frac{\rho_0}{\rho_w}\bar{\mu}\frac{RH}{1-RH}\right)^{-1} \quad (4)$$

where the subscript "*w*" denotes pure water and "0" indicates the dry substance, m_r and m_i are the real and imaginary parts of refractive index. $\bar{\mu}$ is mean linear mass increase coefficient. **Figure 1** shows $\bar{\mu}$ as a function of RH for three aerosol types, which are obtained from the experimental results in **Table 4** of Hänel [10]. As shown, the dependence of $\bar{\mu}$ on RH for difference types of aerosols is rather complicated. RH can affect radiative properties of aerosol particles through changing particle size and refractive index. **Figure 2** shows the changes of densities, refractive indices, and radius for three type aerosols as a function of RH. As shown, the RH effect is important at RH > 80% for density and refractive index, but the radius is sensitive to the change in RH only when RH > 90%.

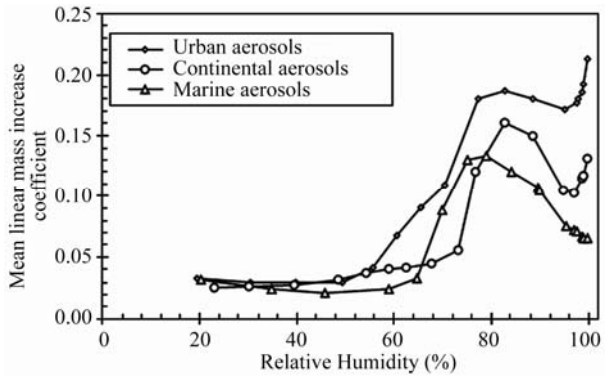

Figure 1. Mean linear mass increase coefficient ($\bar{\mu}$) as a function of relative humidity for three types of aerosols (Maritime aerosols over the Atlantic, 13-16 April, 1969; Urban aerosols at Mainz, January, 1970; Continental aerosols on top of the Hohenpeissenberg, 1000m mean sea level (MSL), summer, 1970) [10].

3. Results and Discussions

3.1. Refractive Index Calculation

One of central questions for prediction of radiative properties of aerosol particles is to accurately calculate their refractive indices. As shown in **Table 1**, the available information on the particle compositions is the ion concentrations of soluble components and compound concentrations of insoluble components. It has been shown that the partial molar refraction approach is applicable to calculate refractive indices for ionic solid-aqueous electrolyte mixtures [14]. The partial molar refraction *R* ($cm^3 \cdot mol^{-1}$) is defined as [15]:

$$R = \frac{n^2 - 1}{n^2 + 2}\left(\frac{M}{\rho}\right) \quad (5)$$

where *n* is refractive index, *M* is molecular weight, and ρ is density ($g \cdot cm^{-3}$). If the molar refractions of components are known, the mean refractive index of a

Copyright © 2011 SciRes.

Table 4. The partial molar refraction of aerosol chemical components. MH [29] is Moelwyn-Hughes [29].

	Species	Partial molar refraction (Ri, cm^{-3})	Ri/Mi	Reference
	Soluble components			
1	H^+	0	0	MH [29]
2	OH^-	4.43	0.261	MH [29]
3	F^-	2.17	0.114	MH [29]
4	Br^-	11.84	0.148	Stelson [14]
5	Cl^-	8.39	0.237	Stelson [14]
6	NO_3^-	10.19	0.164	MH [29]
7	SO_4^{2-}	13.45	0.14	Stelson [14]
8	Na^+	0.93	0.04	Stelson [14]
9	NH_4^+	4.89	0.271	Stelson [14]
10	K^+	3.03	0.078	Stelson [14]
11	Ca^{2+}	1.93	0.048	Stelson [14]
12	Mg^{2+}	0.03	0.001	Stelson [14]
13	$HCOO^-$	7.27	0.161	This work
14	CH_3COO^-	12.94	0.219	This work
15	$CH_3CH_2COO^-$	17.59	0.241	This work
16	$CH_3(CO)COO^-$ (pyruvic)	17.65	0.203	This work
17	$(OOCCOO)^{2-}$ (oxalic)	14.53	0.165	This work
18	$CH_3S(O)_2OH$ (MSA)	16.82	0.175	This work
19	H_2O	3.71	0.206	Stelson [14]
	insoluble component			
20	BC	2.11	0.176	This work
21	SiO_2	7.43	0.124	Stelson [14]
22	Al_2O_3	10.62	0.104	Stelson [14]
23	Fe_2O_3	22.21	0.139	Stelson [14]
24	PbO	18.4	0.082	Stelson [14]
25	Pb	9.24	0.045	Stelson [14]
26	$CH_3(CH_2)_{14}COOH$ (n-Hexadecanoic acid)	78	0.305	This work
27	$CH_3(CH_2)_{16}COOH$ (n-Octadecanoic acid)	87.29	0.307	This work
28	$HOOCCH_2COOH$ (Malonic acid)	17.24	0.166	This work
29	$HOOC(CH_2)_2COOH$ (Succinic acid)	24.2	0.205	This work
30	$HOOC(CH_2)_3COOH$ (Glutaric acid)	28.47	0.216	This work
31	$C_6H_4(COOH)_2$	39.99	0.241	This work
32	other organic compound	50	0.24	This work

medium can be calculated as follows [15]:

$$n = \left[\frac{1 + 2\frac{R}{V}}{1 - \frac{R}{V}} \right]^{\frac{1}{2}} \quad (6)$$

for an aerosol particle:

$$\frac{R}{V} = \frac{\sum \left(\frac{R_i}{M_i} \right) [\mathrm{C}_i]}{[AV]} \quad (7)$$

where R_i is the partial molar refraction of component i in $cm^3 \cdot mol^{-1}$, M_i is the molecular weight of component i in $g \cdot mol^{-1}$, $[C_i]$ is the concentration of component i in $\mu g \cdot m^{-3}$, and [AV] is the aerosol volume in $\mu g \cdot m^{-3}$. The aerosol volume can be either measured or predicted by:

$$[AV] = \sum \frac{\mathrm{C}_i}{\rho_i} \quad (8)$$

where ρ_i is the density of component i in g cm^{-3}. **Table 4**

Copyright © 2011 SciRes.

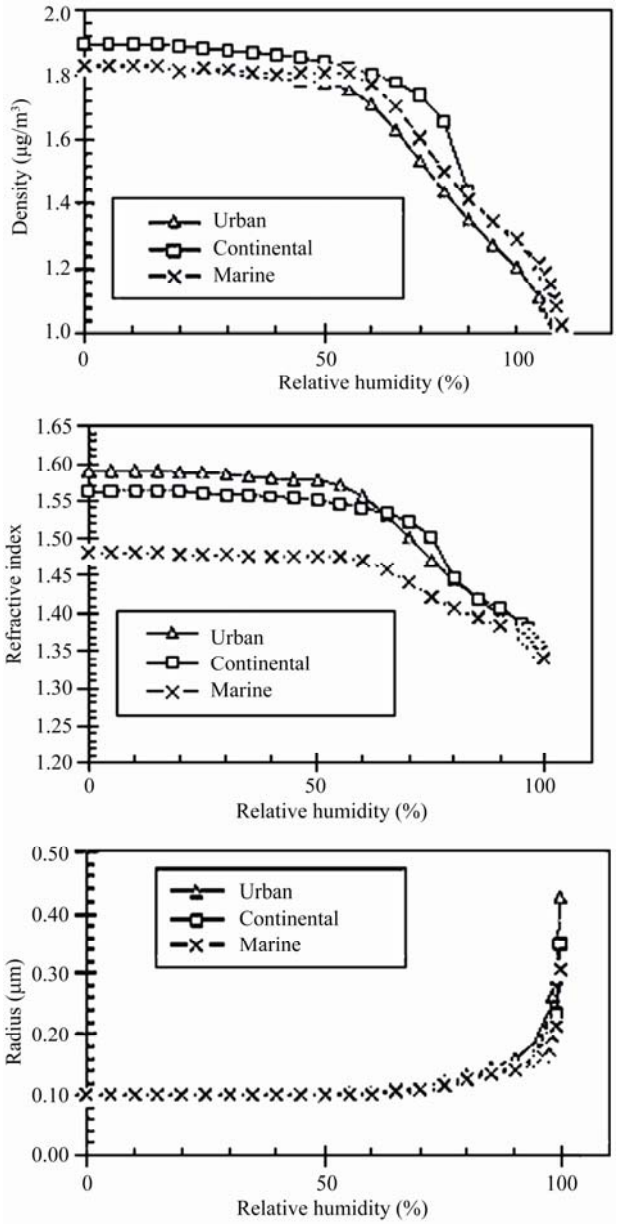

Figure 2. Density, refractive index, and radius as a function of RH for three types of aerosols.

lists the partial molar refractions for ions. **Table 2** contains the refractive index and density for possible salts found in atmospheric aerosol particles. The refractive index and density for most compounds in aerosol particles range from 1.332 to 2.654 and from 0.783 to 11.344 $g \cdot cm^{-3}$, respectively. Volz [16] reported densities of water-soluble materials from different rainfalls and locations to be in a range of 1.76 - 1.96 $g \cdot cm^{-3}$. In this study, the average value (1.86 $g \cdot cm^{-3}$) is used as the mean density for water-soluble parts in aerosol particles. The density (1.40 $g \cdot cm^{-3}$) and refractive index (1.55) for other organic compounds in **Table 2** were taken from the estimates of Sloane [17]. Additionally, the mean aerosol density, ρ, can be calculated from: $\rho = \frac{\sum S_i}{\sum \frac{S_i}{\rho_i}}$.

In this study, the above partial molar refraction approach is extended to calculate the refractive index of any atmospheric particles with the known chemical compositions. **Table 4** lists the partial molar refraction for other aerosol components including insoluble inorganic and organic compounds, which were calculated based on the method of Weast [15]. In this study, an internal mixture is assumed for atmospheric aerosol components. Tang [16] showed that both internal and external mixtures exhibited similar light-scattering properties. **Table 1** lists the values of refractive index and mean density for three typical aerosol types calculated by the partial molar refractive approach. The mean densities for three aerosol types at the dry state range from 1.803 to 1.890 g/m^3. The real parts of refractive index for urban, continental, and marine aerosols are 1.575, 1.557 and 1.479, respectively. As reviewed by Horvath [19], only black carbon (BC, the main constituent of soot) in atmospheric aerosol particles is highly absorbed. Hematite (a-Fe_2O_3) is the only other substance having a light absorption comparable to EC in the near suggest to use full name of "UV", u. v., but absorption rapidly decreases in the visible spectrum of the light. There are some discrepancies about the value of the complex refractive index of EC because of the difficulty of its experimental determination. The values given in the literature range from 1.2 to 2.0 for the real part and from –0.1 to –1.0 for the complex part [19]. In this study, the refractive index used for EC is 2.0 - 0.66i. Since the imaginary parts for all ions in **Table 1** are zero and the densities of each ion in **Table1** are not known, it is not easy to calculate the partial mole refractions of the ions for imaginary parts using the definition equation (5). In this study, the imaginary part of muticomponent aerosols is calculated using the volume average of the imaginary parts of refractive index of the individual species, $\overline{m_i}$, as follows [17]:

$$\overline{m_i} = \left[\sum m_i \frac{S_i}{\rho_i}\right]\left[\sum \frac{S_i}{\rho_i}\right]^{-1}$$

where m_i is the imaginary part of refractive index of component *i*. With the estimates of BC concentration for three types of aerosols in **Table 1**, it was found that the complex refractive indices for urban, continental and marine aerosols are 1.575 – 0.027*i*, 1.557 – 0.016*i*, 1.479 – 0.0027*i*, respectively. Hänel [10] found that the real part of refractive index for urban aerosols in the city of Mainz, Germany, was 1.57 ± 0.04 by actual measurement. Grams *et al*. [20] determined that the complex re-

Copyright © 2011 SciRes.

fractive index for urban aerosols in the city of Boulder, Colorado O, was 1.55 – 0.044*i* on the basis of light scattering measurements. The results from this study are very close to these actual measurements. These complex refractive indices for three types of aerosols will be used in the calculation hereafter.

3.2. The Sensitivity to Relative Humidity

A Mie theory computer code developed by Dave [21] is used in this study to compute aerosol radiative properties. All aerosol particles are assumed to be spherical in shape in the calculation. **Table 3** shows the values of the particle light scattering and extinction coefficients calculated with the above assumption at RHs of 30%, 80% and 99% for different particle size distributions of several aerosol types at a wavelength of 580 nm. The wavelength, 580 nm, is chosen based on the recommendation by Horvath [19] to give the maximum perception of an object under the daylight conditions. As shown, the growth factors for an RH range of 30 to 80% RH range from 1.57 to 1.92 (average 1.77 ± 0.12) and from 1.55 to 1.90 (average 1.77 ± 0.11) for scattering and extinction coefficients, respectively. This is in agreement with the criterion value of the hydroscopic growth factor (1.7 ± 0.3) (which is defined as the ratio of the light scattering coefficient by an aerosol at an RH of 80% to that at 30%) derived from the direct nephelometer measurement [22]. This value has been utilized to date as the first estimate in climate change modeling studies [1]. It is interesting to note that Hegg *et al*. [23] obtained substantially larger values of the hygroscopic growth (see **Table 1** of Hegg *et al*. [23]) for the same size distribution as those in **Table 3**. Hegg *et al*. [23] attributed it to be influenced by the position of the initial dry aerosol size distribution relative to the effective light scattering droplet size range. The main differences in our calculation results and those of Hegg *et al*. [23] lie in different values of the refractive index and mean linear mass increase coefficient used for aerosol particles. The consistence of our results in **Table 3** with the range of hygroscopic growth factor (1.5 to 1.8) from the direct measurements of Charlson *et al*. [22] indicates that our calculation for the effects of RH on scattering coefficient is reasonable. At a high RH such as 99%, the growth factors are much higher and more variable than values at lower RHs as shown in **Table 4**. The growth factors range from 1.06 to 1.18 (average 1.12 ± 0.04) and from 1.10 to 1.53 (average 1.32 ± 0.13) for asymmetry factor in the RH range of 30% to 80% and 30% to 99%, respectively. The growth factors range from 1.01 to 1.06 (average 1.03 ± 0.02) and from 1.02 to 1.14 (average 1.08 ± 0.04) for the single scattering albedo in the RH range of 30% to 80% and 30% to 99%, respectively. The single scattering albedo is not sensitive to RH. At a high RH such as 99%, the single scatter albedo is close to 1.0. The single scattering albedo and asymmetry factor are insensitive to changes in RH. This is in agreement with those of Pilinis *et al*. [24]. Both scattering and extinction coefficients are more sensitive to changes in RH than single scatter albedo and asymmetry factor.

3.3. The Sensitivity to Refractive Index

In the following sensitivity studies, the parameters used for three types of aerosols are assumed to be (1) urban aerosols of Meszaros [25], N=560 cmμm, D_g=0.100 μm, σ_g =2.0, m=1.590 – 0.027*i*, RH = 80%; (2) continental aerosols of Hoppel *et al*. [24], N = 3000 cm^{-3}, D_g = 0.080 μm, σ_g = 2.0, m = 1.564 – 0.016*i*, RH = 80%; (3) marine aerosols of Gathman [27], N = 67 cm^{-3}, D_g=0.266 μm, σ_g = 1.622, m = 1.479 – 0.003*i*, RH = 80%. Note that the values of radius, refractive index in the above assumptions are for a dry state. RH is set to be 80% in the Mie calculation. **Table 5** lists the ranges and averaged values of the change factors for the effects of real and imaginary parts of refractive index on the aerosol radiative properties. The scattering and extinction coefficients increase by about 48% and asymmetry factor decrease by 6% with real part increasing from 1.4 to 1.65. But the single scattering albedo is insensitive to the changes in real part. **Figures 3(a)** and **(b)** show extinction coefficient and single scatter albedo as a function of real part of refractive index for three types of aerosols at a wavelength of 580 nm. **Table 5** shows that the scattering coefficient and single scattering albedo decrease by 18% and 24% when imaginary part varies from –0.005 to 0.10, respectively. The extinction coefficient and asymmetry factor are insensitive to the change in the imaginary part. As expected, extinction coefficient and asymmetry factor increase slightly as imaginary part increases.

3.4. The Sensitivity to Size Distributions

As shown in **Table 5**, scattering and extinction coefficients are very sensitive to changes in geometric mean radius. The scattering and extinction coefficients increase by factors of 118 and 123, respectively, whereas the asymmetry factor only increases by 17% and the single scattering albedo decreases by 0.8%, when the geometric mean radius varies from 0.05 to 0.3 μm. **Figures 4(a)** and **(b)** show the sensitivity tests for the case of marine aerosols at different wavelengths. **Table 5** lists the ranges and averaged changes of radiative properties for three types of aerosols when geometric standard deviation (σ_g) varies from 1.2 to 3.0. The scattering and

Copyright © 2011 SciRes.

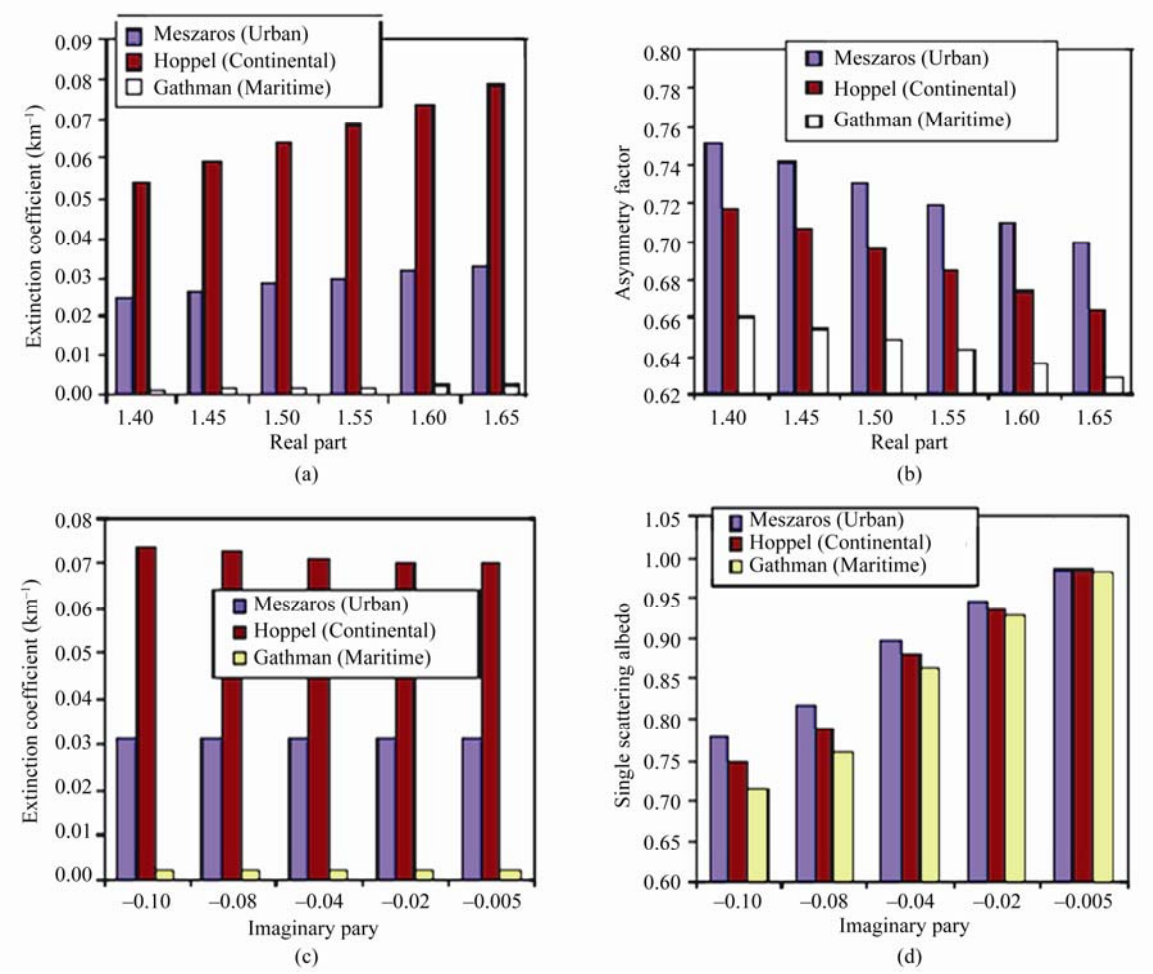

Figure 3. The radiative properties at 580 nm as a function of real and imaginary parts of refractive index for three types of aerosols at a dry state.

Table 5. The change factors for radiative properties of aerosols as a function of real part, imaginary part, geometric mean radius (r_g) and geometric standard deviation (σ_g). The values in parenthesis are the average change factors.

	Real part from 1.40 to 1.65	Imaginary part from –0.005 to –0.10	r_g from 0.05 to 0.3 mm	σ_g from 1.20 to 3.0
Scattering coefficient	1.34-1.65 (1.49)	0.80-0.84 (0.82)	51.5-248.5 (118.8)	153-753 (389)
extinction coefficient	1.32-1.65 (1.47)	1.01-1.15 (1.07)	59.2-249.3 (123.7)	155-607 (334)
Asymmetry factor	0.92-0.95 (0.94)	1.03-1.01 (1.02)	1.09-1.32 (1.17)	3.1-8.3 (5.4)
Single scattering albedo	1.00-1.01 (1.01)	0.79-0.73 (0.76)	0.87-1.00 (0.92)	0.99-1.24 (1.1)

extinction coefficients and asymmetry factor are very sensitive to the change in geometric standard deviation. The scattering and extinction coefficients increase by factors of 389.3 and 334, respectively, when geometric standard deviation varies from 1.2 to 3.0. This change of σ_g results in the increase of asymmetry factor by a factor of 5.4 and the increase of single scattering albedo by 10%. **Figures 4(c)** and **(d)** show the sensitivity of asymmetry factor and single scattering albedo to changes in σ_g values for urban aerosols at different wavelengths. **Figure 5(a)** and **(b)** show the changes of the shape of aerosol size distribution when geometric mean radius varies from 0.1 to 0.4 μm at N_0=560 cm^{-3} and σ_g = 2.0 and when geometric standard deviation varies from 1.2 to 3.0 at N_0 = 560 cm^{-3} and r_g=0.15 μm, respectively. Since the light scattering efficiency of an individual particle is dependent on the particle size, with peak efficiencies occurring between ~0.2 and 0.7 μm in particle radius for a light wavelength of 580 nm, aerosol particles can have large scattering and extinction coefficients if their size distributions grow into this efficient light scattering size range. **Figure 5** indicates that both cases can result

Copyright © 2011 SciRes.

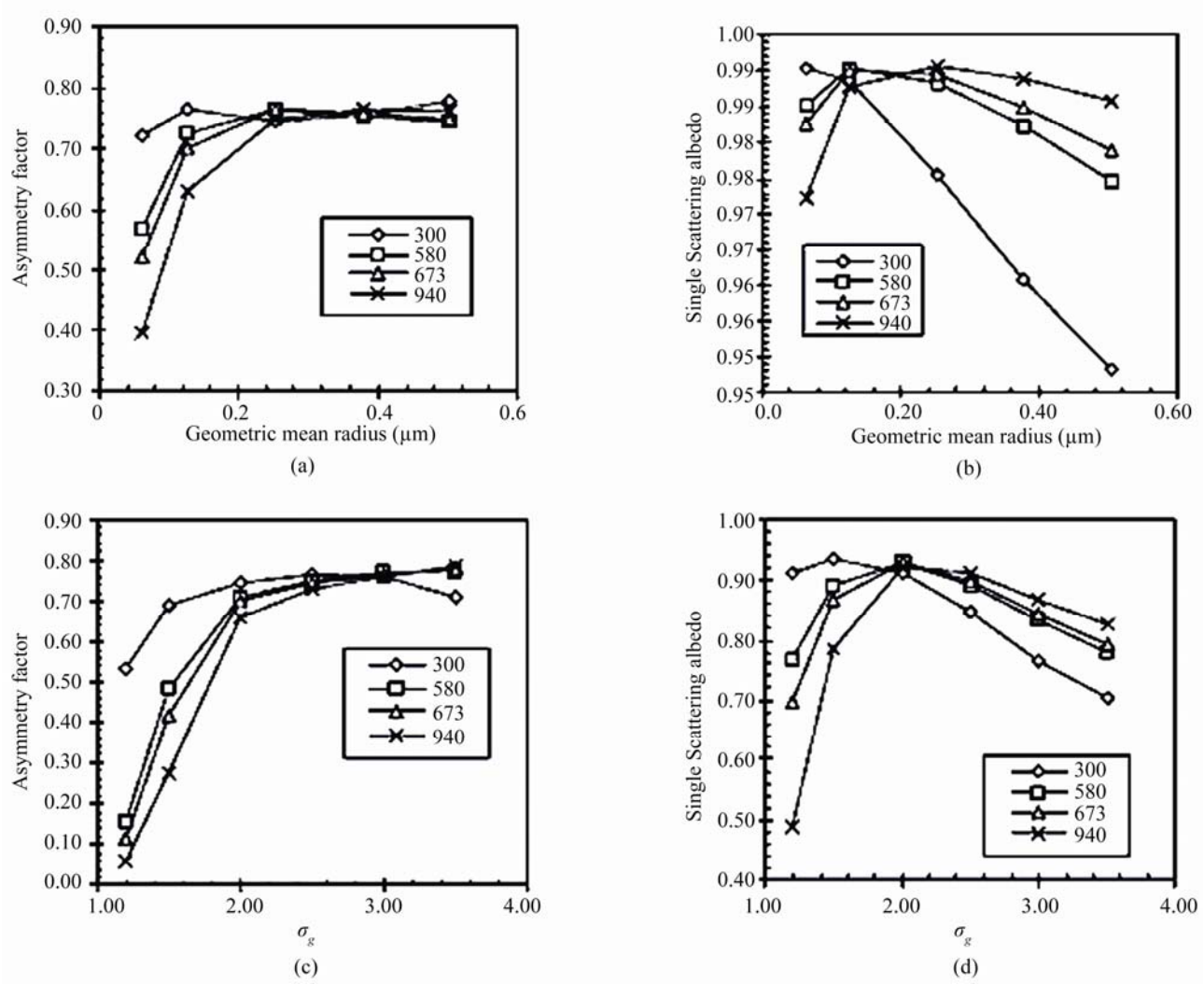

Figure 4. The radiative properties at 580 nm as a function of geometric mean radius (for Gathma's maritime aerosols (a, b), and geometric standard deviation (for Meszaros' urban aerosols (c, d)).

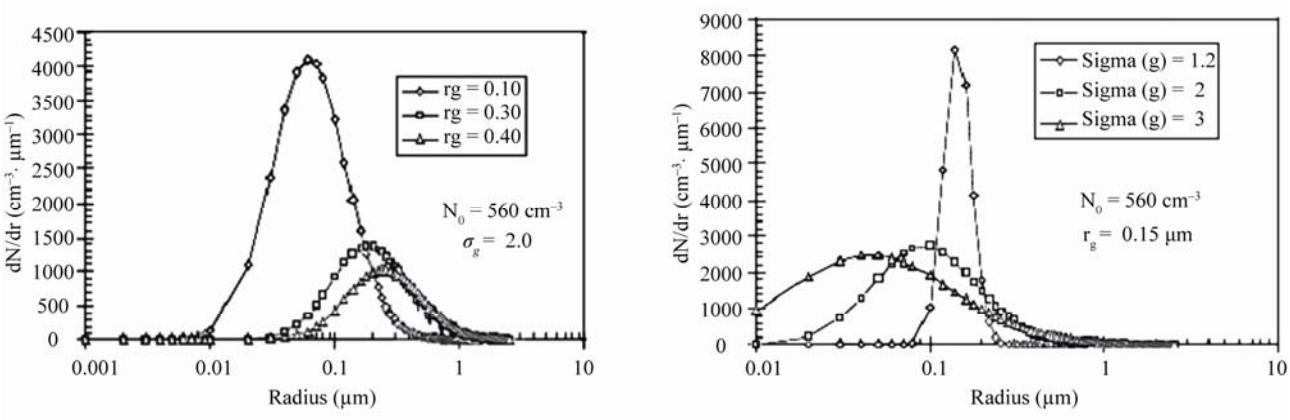

Figure 5. The size distribution of aerosol number concentration as a function of geometric mean radius (a) and standard deviation (b).

Copyright © 2011 SciRes.

in more particles in the efficient light scattering size range (with radii of 0.2 to 0.7 μm). It is not surprised to find that the scattering and extinction coefficients are very sensitive to the changes in geometric mean radius and geometric standard deviation.

3.5. The Sensitivity of Wavelength Dependence of Radiative Properties

The wavelength dependence of aerosol radiative properties is very sensitive to geometric mean radius. When the geometric mean radius is small, both single scattering albedo and asymmetry factor decrease with increasing wavelengths, but when the geometric mean radius becomes larger than a value, both single scattering albedo and asymmetry factor increase with increasing wavelengths. For the latter case, the Angstrom law will not be applicable. The values of geometric mean radii at the crossing point are different for asymmetry factor and single scattering albedo as shown in **Figures 4(a)** and **(b)**, and are also determined by the geometric standard deviation as analyzed below. Since the light scattering efficiency of an individual particle is a nonlinear function of particle size and depends on the particle size and light wavelength tested, and the refractive index is wavelength dependent, the wavelength dependence of aerosol radiative properties will strongly rely on the size distribution and refractive index. For the wavelength dependence of refractive index, available data were closely matched by setting $n(\lambda) = n(\lambda = 0.598\ \mu m) - 0.03(\lambda - 0.598)$, where λ is the wavelength in μm. As shown, the wavelength dependence of refractive index is weak. As shown in **Figure 4**, the wavelength dependence of asymmetry factor and single scattering albedo strongly relies on the geometric mean radius and geometric standard deviation. But the wavelength dependence of scattering and extinction coefficients on the geometric mean radius and geometric standard deviation is weak. For small geometric mean radius and small geometric standard deviation, both asymmetry factor and single scattering albedo increase with decreasing wavelengths, however, for large values of geometric mean radius and geometric standard deviation, both asymmetry factor and single scattering albedo increase with increasing wavelengths, especially for single scattering albedo, as shown in **Figure 4**.

3.6. Radiation Transmission

Since human-induced aerosols are likely to greatly influence future regional climate change instead of global climate change, it is of interest to examine the sensitivity of the aerosol-induced radiation transmission changes at a local or regional scale to aerosol composition, size distributions, and RH. In this study, the radiation transmission is calculated for the assumed aerosol layer with a depth of 2 kilometers using the Madronich's Tropospheric Ultraviolet-Visible Radiation Transfer Model (TUVRTM) [28]. The optical depth $\tau = \int_{z_1}^{z_2} \sigma_e(z)\mathrm{d}z$ is calculated by assuming a constant extinction coefficient within the aerosol layer. The sensitivity of aerosol-induced radiation transmission changes at 580 nm is examined under the following constant conditions: date = 7/01/1995, O_3 = 278 DU, ground albedo = 0.15, air pressure = 940 mb, Latitude = 35.63°, longitude = 82.33°, UT = 17.90, solar zenith angle=13.31, the aerosol layer = 2 km. Three aerosol radiative properties (optical depth, asymmetry factor, and single scattering albedo) are needed in the TUVRTM model to calculate the aerosol-induced radiation transmission changes. In this section, the sensitivity of the aerosol-induced radiation transmission change to RH, refractive index, and size distribution is studied based on previous calculation re-

Table 6. The radiation transmission at 580 nm calculated by a radiative transfer model for different aerosol types assuming an aerosol layer of 2 km. The date is 7/1/1995, O_3 = 278 DU, latitude = 35.63°, longitude = –82.33°, UT = 17.90, zenith angle = 13.31°.

		Accumulation mode			Transmission at 580 nm				
Spectrum	Aerosol types	n (cm^{-3})	D_g (μm)	σ_g	T_1 (RH=30)	T_2 (RH=80)	T_1 (RH=99)	T_2/T_1	T_3/T_1
Meszaros [23]	Urban	560	0.1	2	0.908	0.908	0.906	1	1
Whitby [28]	Continental	2300	0.076	2	0.906	0.906	0.890	1	0.98
Hoppel *et al* [24]	Continental	3000	0.08	2	0.904	0.895	0.840	0.99	0.93
Leaitch and Isaac [29]	Continental	1000	0.24	1.35	0.897	0.895	0.844	1	0.94
Jenning *et al* [30]	Continental-marine mixture	950	0.2	1.35	0.904	0.903	0.876	1	0.97
Gathman [25]	Maritime	67	0.266	1.62	0.911	0.911	0.911	1	1
Jaenicke and Schutz [31]	Polar aerosol	18.6	0.75	2	0.910	0.911	0.911	1	1
Background	without aerosol layer	0	0	0	0.911	0.911	0.911		

Copyright © 2011 SciRes.

Table 7. The change factors for radiation transmission at 580 nm as a function of relative humidity and radiative properties for three types of aerosols. * The average is calculated only for urban and continental aerosols.

	Aerosol type			
Parameter	Urban	Continental	Marine	average*
Relative humidity from 0 to 95%	0.999	0.993	1	0.996
Real part from 1.40 to 1.65	0.998	0.992	1	0.995
Imaginary part from –0.005 to –0.10	0.979	0.967	0.998	0.973
Number concentrations from 50 to 4000 cm^{-3}	0.94	0.977	0.977	0.958
r_g from 0.05 to 0.30 μm	0.467	0.022	0.99	0.244
σ_g from 1.2 to 3.0	0.934	0.831	0.997	0.883

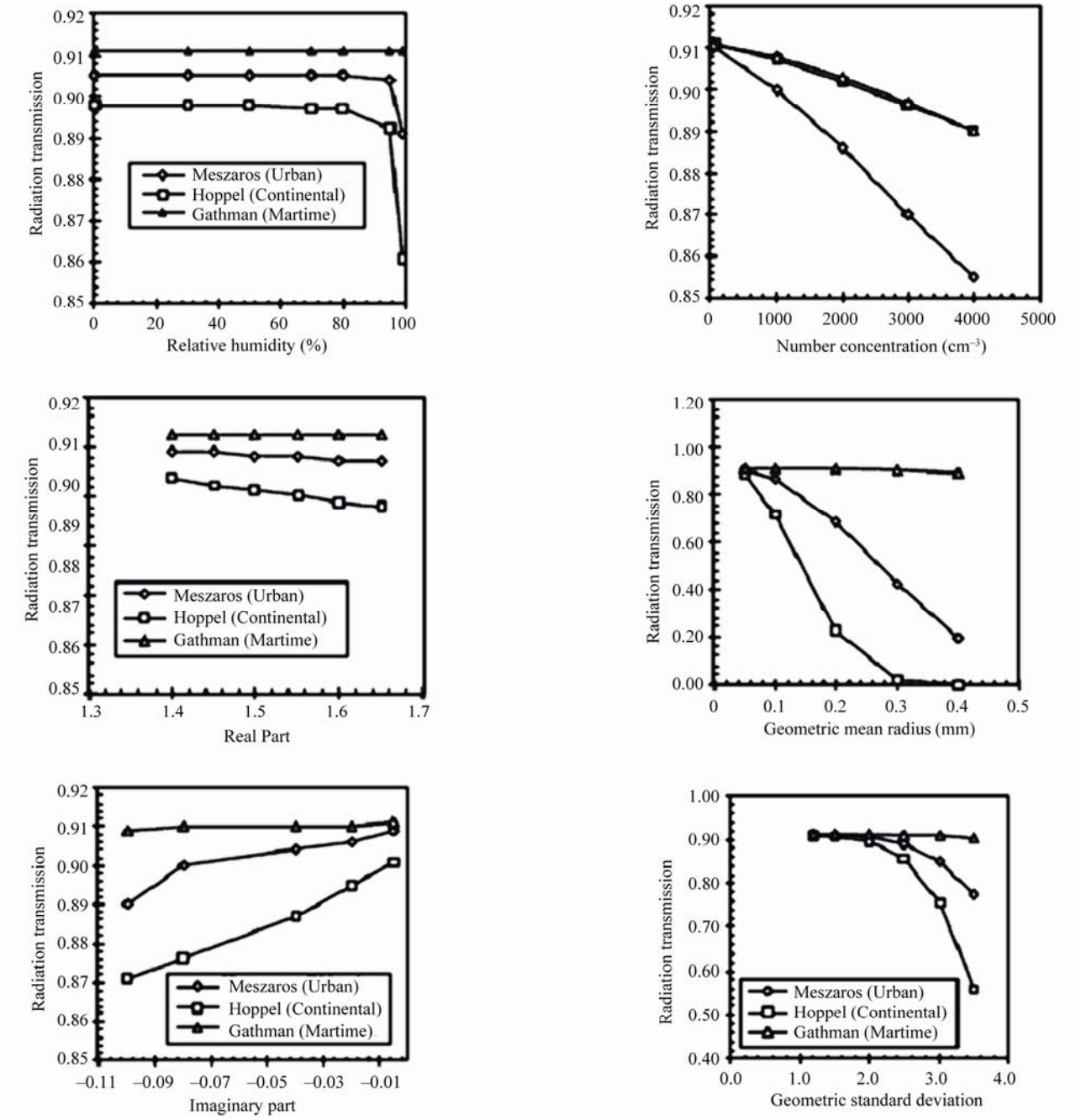

Figure 6. The radiation transmission at 580 nm across an aerosol layer with a 2-km in depth as a function of RH, real and imaginary parts, number concentration, and size distribution for three types of aerosols.

Copyright © 2011 SciRes.

sults of aerosol radiative properties for the three types of aerosols. **Table 6** lists the radiation transmissions at 580 nm for different aerosol types at RHs of 30%, 80% and 99%. **Figure 6** shows the sensitivity of radiation transmission to RH, refraction index, number concentrations and size distributions for the three types of aerosols. **Table 7** lists the change factors for radiation transmission for three types of aerosols. Note that the radiation transmission at 580 nm is 0.911 without the aerosol layer under the assumed atmospheric conditions. It is interesting to note that the radiation transmission is not sensitive to the changes in the above parameters if the total aerosol number concentration is small as it for maritime aerosols of Gathman [27] (total number concentration is only 67 cm^{-3} as indicated in **Table 7**). In this case, the radiation transmission only decreases by 0.4% and 0.5% when RH varies from 0% to 95% and the real part varies from 1.40 to 1.65, respectively. The radiation transmission is sensitive to the change in imaginary part and number concentrations with the decrease of visible radiation transmission by 2.7% and 4.2% when the imaginary part varies from –0.005 to –0.1 and number concentration from 50 to 4000 cm^{-3}, respectively. The radiation transmission is very sensitive to the changes in geometric mean radius and geometric standard deviation. The radiation transmission decreases by 76% when geometric mean radius varies from 0.05 to 0.3 μm and decreases by 12% when geometric standard deviation varies from 1.2 to 3.0. This is in agreement with the strong dependence of scattering and extinction coefficients on geometric mean radius and geometric standard deviation. It should be emphasized that the radiation transmission also strongly depends on the solar zenith angle, latitude and longitude, and ozone concentrations.

4. Conclusions

In this work, the partial molar refraction method is used to accurately calculate the real part of refractive index of aerosol particles with actual measured chemical compositions including soluble inorganic and organic ions and insoluble inorganic and organic substances. It is found that the complex refractive indices for urban, continental and marine aerosols are $1.575 - 0.027i$, $1.557 - 0.016i$ and $1.479 - 0.003i$, respectively. The scattering and extinction coefficients are sensitive to changes in RH, while both single scattering albedo and asymmetry factor are insensitive to change in RH. The extinction coefficient and asymmetry factor are sensitive to changes in real part of refractive index. The scattering coefficient and single scattering albedo are sensitive to the imaginary part changes. The aerosol radiative properties are very sensitive to the change in both geometric mean radius and geometric standard deviation of a particle size distribution. The radiation transmission decreases by 76% and 12% when geometric mean radius varies from 0.05 to 0.3 μm and geometric standard deviation varies from 1.2 to 3.0, respectively. Other sensitivities for the radiation transmissions are insignificant. The comparison between theoretical calculation and actual measurement will be necessary in the future work.

5. References

[1] Charlson R. J., , S.E. Schwartz, J. M. Hales, R. D. Cess, J. A. Coakley, J. E. Hansen, and D. J. Hofmann, Climate forcing by anthropogenic aerosols. *Science*. 225, 423-430, 1992.

[2] Yu, S. C. The role of organic acids (formic, acetic, pyruvic and oxalic) in the formation of cloud condensation nuclei (CCN): A review, *Atmos. Res*., 53, 185-217, 2000

[3] Yu, S. C., V. K. Saxena, and Z. Zhao (2001), A comparison of signals of regional aerosol-induced forcing in eastern China and the southeastern United States, Geophys. Res. Lett., 28, 713-716.

[4] Intergovernmental Panel on Climate Change (IPCC) (2007), Climate Change 2007: The Physical Science Basis, Contribution of Working Group I to the Fourth Assessment Report of the Intergovernmental Panel on Climate Change, Cambridge Univ. Press, New York.

[5] Penner J.E., R. J. Charlson, J. M. Hales, N. S. Laulainen, R. Leifer, T. Novakov, J. Ogren, L. F. Radke, S. E. Schwartz, and L. Travis, Quantifying and minimizing uncertainty of climate forcing by anthropogenic aerosols. *Bull. Amer. Meteorol. Soc*. 75, 375-400, 1994.

[6] Boucher O., and T. L. Anderson, General circulation model assessment of the sensitivity of direct climate forcing by anthropogenic sulfate aerosols to aerosol size and chemistry. *J. geophys. Res*. 100, 26117-26134, 1995.

[7] Jacobson, M. Z., Global direct radiative forcing due to multicomponent anthropogenic and natural aerosols, *J. Geophys. Res*., 106, 1551-1568, 2001

[8] Koch, D., S. Bauer, A. Del Genio, G. Faluvegi, J.R. McConnell, S. Menon, R.L. Miller, D. Rind, R. Ruedy, G.A. Schmidt, and D. Shindell, 2011: Coupled aerosol-chemistry-climate twentieth century transient model investigation: Trends in short-lived species and climate responses. *J. Climate*, doi:10.1175/2011JCLI3582.1, 2010

[9] Rogge, W. F., M. A. Mazurek, L. M. Hildemann, G. R. Cass, and B. R. T. Simoneit, Quantification of urban organic aerosols at a molecular level: Identification, abundance and seasonal variation. *Atmos. Environ*., 27, 1309-1330, 1993.

[10] Hänel G., The properties of atmospheric aerosol particles as functions of relative humidity at thermodynamic equilibrium with the surrounding air. *Adv. Geophys*., 19, 73-188, 1976.

[11] Pueschel R. F., Atmospheric aerosols. In *Composition,*

Copyright © 2011 SciRes.

Chemistry and Climate of the Atmsophere. Ed. Singh H. B.,Van Nostrand Reinhold. pp. 120-175, 1995.

[12] Chylek P., and J. Wong, Effect of absorbing aerosols on global radiation budget. *Geophys. Res. Lett.,* 22, 929-931.

[13] Huntzicker, J.J., Johnson, R.L., Shah, J.J. and Cary, R.A. (1982), Analysis of organic and elemental carbon in ambient aerosols by a thermal-optical method. In *Particulate Carbon: Atmospheric Life* using a particle trap impactor/denuder sampler. *Environ. Sci. Technol.* 35(24):4857-4867.

[14] Stelson A. W., Urban aerosol refractive index prediction by partial molar refraction approach. *Environ. Sci. Technol*., 24, 1676-1679, 1990.

[15] Weast R. C., CRC Handbook of Chemical and Physics, Cleveland, OH, 1988.

[16] Volz F., Infrared absorption by atmsopheric aerosol substances. *J. geophys. Res*. 77, 1017-1031, 1972.

[17] Sloane C. S., Optical properties of aerosols of mixed composition. *Atmos. Environ*., 18, 871-878, 1984.

[18] Tang I. N., W.T. Wong, and H.R. Munkelwiz., The relative importance of atmospheric sulfates and nitrates in visibility reduction. *Atmos. Environ*., 15, 2463-2471, 1981.

[19] Horvath H., Atmospheric light absorption-a review. *Atmos. Environ*. 27, 293-317, 1993

[20] G.W. Grams, I.H. Blifford, D.A. Gillette and P.B. Russell, Complex index of refraction of airborne soil particles, *J. appl. Met.* 13 (1974), pp. 459-471

[21] Dave J. V., Subroutines for computing the parameters of electomagnetic radiation scattered by a sphere. IBM J. Res. Dev., 13, 302-312, 1969.

[22] Charlson R. J., D. S. Covert, and T. V. Larson, Observations of the effect of humidity on light scattering by aerosols, in *Hygroscopic Aerosols,* edited by Ruhnke T. H. and Deepak A. pp 35-44, A. Deepak, Hampton, VA, 1984.

[23] Hegg D., T. Larson ,and P. F. Yuen, A theoretical study of the effect of relative humidity on light scattering by tropospheric aerosols. . *J. geophys. Res*. 98, 18435-18439, 1993.

[24] Pilinis C., S. N. Pandis, and J. H. Seifeld, Sensitivity of direct climate forcing by atmospheric aerosols to aerosol size and composition. *J. geophys. Res*. 100, 18739-18754, 1995.

[25] Meszaros A., On the concentration and size distribution of atmospheric sulfate particles under rural conditions. *Atmos. Environ*. 12, 2425-2428, 1978.

[26] Hoppel W. A., R. Larson and M. A. Vietti. Aerosol size distributions at a site on the east coast of the United States. *Atmos. Environ*. 18, 1613-1621, 1984.

[27] Gathman S. C., Optical properties of the maritime aerosols as predicted by the Navy aerosol model. Opt. Engineer, 22, 56-62, 1983.

[28] Madronich, S. 1993. Tropospheric photochemistry and its response to UV changes. In *The role of the stratosphere in global change*. Vol. 18. NATO-ASI Series, ed. M-L. Chanin, 437-61. Amsterdam: Springer-Verlag

[29] Moelwyn-Hughes E. A., Physical chemistry, 2nd rev. ed.; Pergamon Press, New York, 1961

[30] Whitby K. T., The physical characteristics of sulfur aerosols. *Atmos. Environ*., 12, 135-159, 1978.

[31] Leaitch W. R. and G. A. Isaac, Tropospheric aerosol size distributions from 1982 to 1988 over eastern North America. *Atmos. Environ*. 25, 601-619, 1991.

[32] S.G. Jennings, C.D. O'Dowd, T.C. O'Connor and F.M. McGovern, Physical characteristics of ambient aerosol at Mace Head. *Atmospheric Environment* 25A (1991), pp. 557-562.

[33] Jaenicke, R. and Schiitz, L. 1982. Arctic aerosol in surface air. *ldoyaras* 86, 235-241.

Copyright © 2011 SciRes.